Atmos. Chem. Phys. Discuss., 14, 10135–10166, 2014
www.atmos-chem-phys-discuss.net/14/10135/2014/
doi:10.5194/acpd-14-10135-2014

Atmospheric Chemistry and Physics Discussions

The influence of nitrogen oxides on the activation of bromide and chloride in salt aerosol

S. Bleicher[1], J. C. Buxmann[2,*], R. Sander[3], T. P. Riedel[4], J. A. Thornton[4], U. Platt[2], and C. Zetzsch[1]

[1]Atmospheric Chemistry Research Unit, University of Bayreuth, Bayreuth, Germany
[2]Institut für Umweltphysik, University of Heidelberg, Heidelberg, Germany
[3]Air Chemistry Department, Max-Planck Institute for Chemistry, Mainz, Germany
[4]University of Washington, Seattle, USA
[*]now at: Met Office, Exeter, UK

Received: 6 March 2014 – Accepted: 11 March 2014 – Published: 22 April 2014

Correspondence to: C. Zetzsch (cornelius.zetzsch@uni-bayreuth.de)

Published by Copernicus Publications on behalf of the European Geosciences Union.

Abstract

Experiments on salt aerosol with different salt contents were performed in a Teflon chamber under tropospheric light conditions with various initial contents of nitrogen oxides (NO_x = NO + NO_2). A strong activation of halogens was found at high NO_x mixing ratios, even in samples with lower bromide contents such as road salts. The ozone depletion by reactive halogen species released from the aerosol, was found to be a function of the initial NO_x mixing ratio. Besides bromine, large amounts of chlorine have been released in our smog chamber. Time profiles of the halogen species Cl_2, Br_2, $ClNO_2$, $BrNO_2$ and BrO, ClO, OClO and Cl atoms were simultaneously measured by various techniques (chemical ionization mass spectrometry, differential optical absorption spectrometry coupled with a multi-reflection cell and gas chromatography of hydrocarbon tracers for Cl and OH, employing cryogenic preconcentration and flame ionization detection). Measurements are compared to calculations by the CAABA/MECCA 0-D box model, which was adapted to the chamber conditions and took the aerosol liquid water content and composition into account. The model results agree reasonably with the observations and provide important information about the prerequisites for halogen release, such as the time profiles of the aerosol bromide and chloride contents as well as the aerosol pH.

1 Introduction

Due to their high reactivity, bromine and chlorine have a strong impact on the chemistry of the atmosphere. In contrast to the situation in the stratosphere, their presence in the troposphere seems to be dominated by natural sources such as sea spray. Especially chlorinated species are difficult to measure directly, resulting in a challenge to infer a budget of total reactive chlorine in the lower atmosphere. Recent studies suggest that a significant fraction of the tropospheric $Cl^{\bullet}$ source is anthropogenic (Thornton et al., 2010). Although the mechanisms of halide activation, namely the conversion of inactive

ACPD
14, 10135–10166, 2014

halides into reactive halogen species (e.g. halogen oxides), are not fully understood, it is known that the pH-value (Betts and Mackenzie, 1951; Fickert et al., 1999; da Rosa and Zetzsch, 2001) and the bromide to chloride ratio (Behnke et al., 1999) have an impact on the activation cycles. Especially the role of NO_x molecules is under discussion. Recently, Lopez-Hilfiker et al. (2012) and Wren et al. (2013) found the production of gaseous chlorine and bromine molecules from NaCl/NaBr-doped and acidified ice surfaces, which was also observed in nature (Pratt et al., 2013) The acidification of such ice surfaces and aerosol droplets can be caused by nitrogen oxides, in particular by the production of N_2O_5 during nighttime and its hydrolysis and dissociation to H^+ and NO_3^- on aqueous surfaces (George et al., 1994; Schütze et al., 2002):

$$NO_3 + NO_2 \rightarrow N_2O_5 \quad \text{(R1)}$$

$$N_2O_5 + H_2O \rightarrow 2HNO_3 \quad \text{(R2)}$$

Nitric acid can also be formed during daytime by the reaction of NO_2 with OH (e.g. Hippler et al., 2006):

$$NO_2 + OH + M \rightarrow HNO_3 + M \quad \text{(R3)}$$

However, the first halogen molecules (indicated by X or Y = Cl, Br) can be activated by dissolved ozone (aqueous species are indicated by "aq") even during nighttime (e.g. Hunt et al., 2004):

$$O_3 \rightarrow O_3(aq) \quad \text{(R4)}$$

$$O_3(aq) + X^- \rightleftharpoons XO^- + O_2 \quad \text{(R5)}$$

$$XO^- + H^+ \rightleftharpoons HOX(aq) \quad \text{(R6)}$$

$$HOX(aq) + H^+ + X^- \rightarrow X_2(aq) + H_2O \quad \text{(R7a)}$$

$$HOX(aq) + H^+ + Y^- \rightarrow XY(aq) + H_2O \quad \text{(R7b)}$$

ACPD
14, 10135–10166, 2014

$$X_2(aq) \rightarrow X_2. \quad \text{(R8)}$$

During the daytime the gaseous halogen molecules are photolyzed to two halogen atoms, which rapidly react with ozone:

$$X_2 + h\nu \rightarrow 2X \quad \text{(R9)}$$

$$X + O_3 \rightarrow XO + O_2 \quad \text{(R10)}$$

The formed bromine oxide is known to effectively deplete ozone catalytically due to its self-reaction:

$$2BrO \rightarrow 2Br + O_2 \quad \text{(R11a)}$$

$$\rightarrow Br_2 + O_2 \quad \text{(R11b)}$$

The branching ratio of Reactions (R11a)/(R11)(overall) is reported to be ~ 0.85 and formation of OBrO and Br is considered to be unimportant (Atkinson et al., 2007). However, under the influence of light Br_2 is photolyzed rapidly (photolysis rates can be found in the Supplement). In the mixed case of additional activated chlorine, the depletion of ozone is even faster. Then BrO may also react with ClO to form a Br atom and an intermediate OClO molecule. OClO in turn reacts with chlorine atoms back to ClO:

$$BrO + ClO \rightarrow OClO + Br \quad \text{(R12a)}$$

$$\rightarrow ClOO + Br \quad \text{(R12b)}$$

$$\rightarrow BrCl + O_2 \quad \text{(R12c)}$$

$$OClO + Cl \rightarrow 2ClO \quad \text{(R13)}$$

XO radicals may also react with hydroperoxyl radicals to form hypohalide acids, which are the driver of Reaction (R7) after their uptake into the aqueous phase:

$$XO + HO_2 \rightarrow HOX + O_2 \quad \text{(R14)}$$

$$HOX \rightarrow HOX(aq) \quad \text{(R15)}$$

ACPD
14, 10135–10166, 2014

The aquatic uptake of one molecule containing one halogen atom and the subsequent release of one molecule containing two halogen atoms into the gas phase results in a self-accelerating autocatalytic activation of halides and thus is called "halogen explosion" (Platt and Janssen, 1995; Hönninger et al., 2004). Under remote conditions the halogen explosion occurs rather for X = Br than for X = Cl. One reason is the faster uptake of HOBr compared to HOCl, due to the higher pK_a value of HOBr (pK_a = 7.8 at 273 K for HOCl, (Morris, 1966), and a pK_a = 8.6 at 274 K for HOBr, Shilov, 1938). Additionally the release of X,Y = Br is favored over X = Cl and Y = Br or X,Y = Cl due to water phase reaction constants (Fickert et al., 1999). In polluted areas the activation can be accelerated by XNO_3, which accrues in the reaction of XO and NO_2 (Cox and Lewis, 1979; Sander et al., 1981):

$$XO + NO_2 + M \rightarrow XNO_3 + M \quad \text{(R16)}$$

$$XNO_3 \rightarrow XNO_3\,(aq) \quad \text{(R17)}$$

$$XNO_3\,(aq) + H_2O \rightarrow HOX\,(aq) + H^+ + NO_3^- \quad \text{(R18)}$$

XNO_3 have a faster uptake to the aqueous phase than HOX (e.g. Hanson et al., 1996; Deiber et al., 2004) and its hydrolysis also provides protons needed by Reaction (R7).

Additionally, heterogeneous reactions are known to influence the halogen chemistry (summarized by Rossi, 2003). E.g. the uptake of N_2O_5 on halide aqueous phase leads to a direct transition of the halides to gaseous photolabile reservoir species (e.g. George et al., 1994):

$$N_2O_5 + X^-\,(aq) \rightarrow XNO_2 + NO_3^-\,(aq) \quad \text{(R19)}$$

This heterogeneous activation mechanism was originally proposed and investigated by Finlayson-Pitts et al. (1989) and confirmed in an aerosol smog chamber by Zetzsch and Behnke (1992) and Behnke et al. (1993, 1997) for chlorine and investigated in detail in a wetted-wall flow-tube by Frenzel et al. (1998), including X = Br. The production of ClNO2 has been observed by Osthoff et al. (2008) in the polluted subtropical marine boundary layer. It alters. The production of $ClNO_2$ alters the NO_x and Cl budgets, both

ACPD
14, 10135–10166, 2014

of which affect the troposphere's oxidizing capacity. Recently, a few hundred ppt of $ClNO_2$ have been measured in the middle of North America (Boulder, Colorado) by Thornton et al. (2010) and over continental Europe (Phillips et al., 2012). A further important class of heterogeneous reactions provides chloride to the aqueous phase example such as the well-known conversion of molecular chlorine to bromine on halide surfaces: One example is the well-known conversion of molecular chlorine to bromine on halide surfaces:

$$Cl_2 + Br^-(aq) \rightarrow BrCl(aq) + Cl^-(aq) \quad \text{(R20)}$$

$$BrCl(aq) + Br^-(aq) \rightleftharpoons Br_2Cl^-(aq) \quad \text{(R21)}$$

$$Br_2Cl^-(aq) \rightarrow Br_2 + Cl^-(aq) \quad \text{(R22)}$$

and the formation of HONO from an uptake of NOCl into the aqueous phase (Scheer et al., 1997):

$$NOCl + H_2O \rightarrow HONO + Cl^-(aq) + H^+(aq) \quad \text{(R23)}$$

Uptake of $ClNO_2$ is possible as well (Behnke et al., 1997), but at a slower rate compared to NOCl (Frenzel et al.,1998). The most important source of NOCl is the reaction of 2 NO_2 + NaCl → NOCl + $NaNO_3$ (Finlayson-Pitts, 1983). A further minor source is the reaction of chlorine atoms with nitrogen monoxide (2.19×10^{-12} cm^3 $molecule^{-1}$ s^{-1}; DeMore et al., 1997).

2 Instrumental setup and methods

The experiments were performed in a 3.7 m^3 Teflon chamber (FEP 200A, DuPont) with a surface to volume ratio of 3.5 m^{-1}. In this chamber we are able to simulate the mixed aqueous and gaseous chemistry of the tropospheric mixed boundary layer (see also Bleicher, 2012). The light of seven medium pressure arc lamps (7 × 1200 W, Osram HMI1200GS) below the chamber is filtered by glass (Schott, Tempax, 3 mm thickness)

ACPD
14, 10135–10166, 2014

and a water layer of 2 cm depth to achieve tropospheric light conditions (see Fig. 1 and appendix for photolysis frequencies). The lamps of this solar simulator have a heat-up phase after ignition lasting for three minutes and causing an increase of intensity and a shift of the spectrum. To avoid an influence on the experiment, the solar simulator was shuttered for the first minutes after ignition. The shutter was removed promptly after the heat-up. The chamber was filled with zero air, containing less than 500 ppt of NO_x and ~ 500 ppb of CH_4. A slight overpressure (around 0.5 Pa), measured by a differential pressure sensor (Kalinsky Elektronik DS1) and controlled by a clean air flow system, diminished the intrusion of ambient air. Since the chamber volume is dependent on the overpressure, the volume specified above was measured at 0.5 Pa differential pressure by knowing the dilution flow and measuring the depletion of an inert tracer like methane in the dark (Bendix hydrocarbon analyzer, model 8201) or n-perfluorohexane.

The temperature and the relative humidity (RH) were measured at three heights (Driesen + Kern DKRF400X-P). The salt aerosol was generated by an ultra-sonic nebulizer (Quick Ohm QUV-HEV FT25/16-A, 35 W, 1.63 MHz) at RH > 50 %. The nebulized stock solution of bi-distilled water contained 1 g L^{-1} NaCl (Sigma-Aldrich, > 99 %, < 0.01 % NaBr) and various concentrations of NaBr (Merck, Suprapur) ranging from 0.42 to 86.4 mg L^{-1}. According to the Köhler theory (e.g. Wex et al., 2005) the concentration of salt in the stock solution determines the aerosol particle diameter to about 400 nm, with resulting ion concentrations of 6.1 mol L^{-1} of chloride and 1.5 to 300 mmol L^{-1} of bromide. The particle size distributions were measured by a particle classifier (TSI, 3071) with a ^{85}Kr neutralizer and a condensation nucleus counter (TSI, 3020) with custom written software for scanning the size distributions and for correction for multiple charges (see also Balzer, 2012). Typical particle distributions are shown in Fig. 2. Higher salt concentrations would lead to bigger particles and thus to a faster sedimentation (Siekmann, 2008). For the given particle diameter we found a lifetime ($1/e$-time) of ca. 5.5 h in our chamber by neglecting a coagulation loss for these large particle sizes. Since the particles were liquid at the given RH, their total volume equals to the liquid water content (lwc, given in $m^3\,m^{-3}$). We have to note that sedimented

ACPD
14, 10135–10166, 2014

aerosol, although not measurable, contributes to the chemistry, which results in a considerable uncertainty for the computer modeling applied in this study. A comparable chamber set-up and the wall effects on the chemistry are also discussed in a recent paper by Hoch et al. (2014).

During the experiments, the bromide concentration was varied for two reasons: (a) the influence of bromide on the activation of chloride by recombination of HOBr(aq) with chloride to BrCl instead of Br_2 in mechanism Reaction (R7), (b) the light loss due to the Mie-scattering by the aerosol within the light path of the differential optical absorption spectrometer (DOAS). While the efficiency of mechanism (a) is a scientific question (b) has a technical origin. The DOAS system has already been described in detail by Buxmann et al. (2012) and Buxmann (2012), and here we give a short overview. The instrument was equipped with a multi-reflection cell (White, 1976) with a base length of 2 m diagonal through the chamber using highly reflective dielectric mirrors (Layertec, $R > 0.995$ between 335 and 360 nm) to achieve a path length of 288 m. This led to a mean BrO and OClO detection limit of 40 ppt and 150 ppt, respectively. The 4σ statistical error of a single spectral fit was taken as an estimate of the detection limit. Optional broadband aluminum mirrors ($R \sim 0.90$ between 300–405 nm) were used to observe a larger variety of species e.g. ClO, O_3 and HONO albeit at a shorter light path. For ClO the chosen light path of 32 m results in a detection limit of $\sim$ 800 ppt. The integrated output light intensity after passing the White cell is proportional to the integration time of the DOAS spectra and thus influences the sensitivity. To minimize light loss, we used low aerosol concentrations (lwc $\sim 5 \times 10^{-10}$) with high bromide content (300 mmol L^{-1}) as compensation in all experiments where DOAS was applied. Ozone was generated by an electrical discharge (Sorbios, GSG 12) in oxygen (Rießner Gase, 99.996 %) and measured by UV absorption (Thermo Scientific, 49i). NO_2 was injected from gas cylinders (Rießner Gase, 101 ppm in N_2) and measured by chemiluminescence (Ecophysics, CLD 88p, CLD 700) with two types of converters: a photolytic converter (Ecophysics, PLC 860, mainly sensitive to NO_2) and a molybde-

ACPD
14, 10135–10166, 2014

num converter (used in the CLD 700 instrument), which is sensitive to a broad spectrum of NO_x species.

The measurement of the ozone temporal variation allows us to estimate the BrO concentration assuming that Reaction (R10) is the dominant O_3 loss process and Reaction (R11a) is the rate-limiting step:

$$-\frac{d[O_3]}{dt} = 2k_1[BrO]^2 + c \quad (1)$$

where c represents other ozone sinks and $k_1 = 2.7 \times 10^{-12}\,cm^3\,molecule^{-1}\,s^{-1}$ is the second order rate constant of Reaction (R11a). In an empty, but humidified and illuminated chamber we observe a typical ozone loss of max. $0.02\,ppb\,s^{-1}$ at ozone mixing ratios below 1 ppm. This value includes a wall loss of max. $\sim 0.015\,ppb\,s^{-1}$ at typical O_3-mixing ratios in the chamber and a humidity dependent loss due to the $O(^1D)$ photolysis channel of ozone. To estimate the BrO mixing ratio from Eq. (1), we eliminated the separately measured dilution rate (but not the wall loss) and removed the noise from the ozone curve by smoothing it using the Savitzky–Golay algorithm.

Hydrocarbons (HC), which can be important sinks for reactive halogens, were measured by gas chromatography (Siemens Sichromat 2, Al-PLOT column 50 m, flame ionization detector, with custom built nitrogen cold trap enrichment). By measuring the decay of a special injected HC mixture (*n*-pentane, 2,2-dimethylbutane, 2,2,4,4-tetramethylbutane, toluene) and an inert dilution standard (*n*-perfluorohexane) we could indirectly determine the concentrations of OH and Cl radicals. This method is known as the radical clock method (RCM, Zetzsch and Behnke, 1992). It was used in selected experiments only since the HC species influence the halogen chemistry. The measured HC time profiles were interpolated by appropriate exponential and/or sigmoidal functions. The time derivatives of the fitted functions allow us to solve the set of n linear equations (n = count of HC species) to get the both unknowns [Cl] and [OH]

ACPD
14, 10135–10166, 2014

for all experimental times t:

$$\frac{\mathrm{d}[\mathrm{HC}]_i}{\mathrm{d}t} = -k_{\mathrm{OH},i}[\mathrm{OH}][\mathrm{HC}]_i - k_{\mathrm{Cl},i}[\mathrm{Cl}][\mathrm{HC}]_i, \quad (i = 1, \ldots, n) \tag{2}$$

This technique was also employed to determine the solar simulator's actinic photon flux in the UV range by chlorine actinometry. UV light below 330 nm has a high impact on the chemistry by forming excited state oxygen atoms and hence OH radicals by ozone photolysis. In this spectral region the chlorine actinometry is more precise than the NO_2 actinometry, since the chlorine molecule has a broad absorption maximum in the UV with its maximum at 330 nm (e.g. Maric et al., 1993). In the irradiated chamber, the behavior of chlorine atoms basically follows the equation:

$$\frac{\mathrm{d}[\mathrm{Cl}]}{\mathrm{d}t} = 2j(\mathrm{Cl_2})[\mathrm{Cl_2}] - \sum_i k_{\mathrm{Cl},i}[\mathrm{Cl}][\mathrm{HC}]_i, \quad (i = 1, \ldots, n) \tag{3}$$

where photolysis of Cl_2 is the source and the I reactions with hydrocarbons are the sinks of atomic Cl. Assuming that the photolytic decay of Cl_2 is exponential and neglecting the time dependence of HC_i as a simplification (which is reasonable since the HC are in excess) we are able to solve Eq. (3) analytically. The solution is a bi-exponential function of time with $j(Cl_2)$ and $[Cl_2]_{t=0}$ as parameters. Using the obtained $j(Cl_2) = 2.4 \times 10^{-3}\,s^{-1}$ we normalize the previously measured lamp spectrum by the chlorine photolysis frequency (Fig. 1). The $j(NO_2) = 6.7 \times 10^{-3}\,s^{-1}$ values derived from Cl_2 photolysis were found to agree with NO_2 actinometry ($j(NO_2) = 7.1 \times 10^{-3}\,s^{-1}$) within an acceptable deviation of less than 6 %.

Additionally used in a measurement campaign was a chemical ionization mass spectrometer (CIMS), which was described by Kercher et al., 2009 to observe non-radical species. All instruments, except the GC, were connected to the chamber by Teflon tubes as short as possible with (1–3 m length). Chemical conversion of highly reactive bromine compounds like BrO or HOBr on instrument and inlet surfaces is a well known

ACPD
14, 10135–10166, 2014

problem and can even result in a complete loss of BrO (Neuman et al., 2010). Therefore it is important to keep the inlet short, as it was demonstrated by Liao et al. (2011).

We compared our measurements to simulations with version 3.0 of the chemical box model CAABA/MECCA (Chemistry As A Boxmodel Application/Module Efficiently Calculating the Chemistry of the Atmosphere) by Sander et al. (2011). The model was run for 144 min, with output every 6 s. To represent our laboratory conditions, the "LAB" scenario in the model was set to $T = 293\,\mathrm{K}$, $p = 101\,325\,\mathrm{Pa}$, and a RH of 60 %. The modeled aerosol has a liquid water content of $5 \times 10^{-9}\,\mathrm{m^3\,m^{-3}}$ and contains particles with a radius of 0.2 µm. In addition to the standard ozone, methane, HO_x, and NO_x chemistry, we activated chlorine and bromine multiphase chemistry in the gas phase and in the aerosol particles. A list of the chemical reactions used in this study, including rate coefficients and references, is available in the Supplement. Photolysis frequencies were calculated for the solar simulator by building a scalar product of the spectrum shown in Fig. 1 and the cross sections of the molecules weighted by the quantum efficiencies. All photolysis values are scaled with a single factor which represents the age of the lamps (a new lamp has ca. four times more intensity than an old lamp with more than 600 operating hours). The photolysis frequencies and the scaling factor were kept constant during the whole model simulation. For ozone, a constant destruction term of $1.3 \times 10^{-5}\,\mathrm{s^{-1}}$ represents wall losses. The gas phase was initialized with $500\,\mathrm{nmol\,mol^{-1}}$ CH_4, while the ozone and NO_x mixing ratios were adapted to the conditions of individual experiments. The initial composition of the aerosol was $6.1\,\mathrm{mol\,L^{-1}}$ chloride and $0.3\,\mathrm{mol\,L^{-1}}$ bromide. The model in its original state overpredicts the concentrations of HOX species on the cost of the XO compared to the results gained from the DOAS and the CIMS experiments (see Sect. 3). We assume that the chamber walls act as a source of active halogens due to the deposits of HX from previous experiments. After testing various possibilities to include a simplified wall source Q, such as $HOX + Q \rightarrow X_2$, we found that the addition of two reactions to the model $HOX \rightarrow X + OH$ ($k = 0.12\,\mathrm{s^{-1}}$ for X = Br and $0.02\,\mathrm{s^{-1}}$ for X = Cl) results in a good agreement with the experimental data over a wide range of initial ozone and NO_x mixing ratios. Although the

ACPD
14, 10135–10166, 2014

constants are fast, this approximation is conservative since it does not add halogens to the system.

3 Results and discussion

From a series of experiments with various initial NO_x-mixing ratios we discuss four experimental runs in detail: two experiments (which are quite comparable in almost all parameters except their initial NOx mixing ratio) with the DOAS instrument and two experiments with the CIMS instrument.

3.1 Low NO_x experiment with DOAS

The first experiment (Fig. 3) is a low NO_x-case. Before starting the experiment, by injection of the salt aerosols, the chamber was cleaned photochemically by introducing high levels of humidity (> 60 %) and ozone (~700 ppb) and UV radiation of our solar simulator. Therefore the possibility of remaining organic from former experiments and additional wall release of BrO was minimized during the actual experiment. Here we nebulized a stock solution of 86.4 mg L^{-1} NaBr and 1 g L^{-1} NaCl into a humid chamber (50 % rel. humidity at 293 K), which should result in a bromide concentration of 300 mmol L^{-1} and 6.1 mol L^{-1} chloride in the aerosol phase according to the Köhler theory. The particle concentration reached 1650 cm^{-3}, containing 7×10^{-11} m^3 m^{-3} of liquid water. The particle size distribution is shown in Fig. 2a. The bromide concentration per cm^3 could allow a maximal Br_x mixing ratio of 515 ppt in case of its entire activation. The nighttime chemistry (R1, R2 and R19) started by injection of ozone (508 ppb), which induces a complete loss of the initial NO_2 mixing ratio of 500 ppt. The ozone mixing ratio was nearly constant with a (dilution-corrected) loss rate of less than -0.01 ppb s^{-1} in the dark.

We switched the solar simulator on at $t = 0$. The loss of ozone accelerated in the day time conditions and reached a peak value of -58 ppt s^{-1} after 30 min of illumination. As

ACPD
14, 10135–10166, 2014

expected, the measured BrO concentration was correlated to the O_3-derivative (slope of the ozone time profile); the peak of [BrO] = 300 ± 85 ppt is coincident with the O_3 depletion maximum. A fraction of the observed BrO was released by the chamber walls in a previous high ozone chamber purge without aerosol and remained as a stable background level of 200 ppt of BrO in the chamber during the dark phase. Thus, from the BrO-mixing ratio an offset of 200 ppt was subtracted, since it was obviously an artefact remaining after the previous chamber purge. During the cleaning phase remaining organic, has been detected in form of formaldehyde by the DOAS-instrument. The formaldehyde signal was below the mean detection limit of ~60 ppb, once we started the salt aerosol experiment. In this experiment, the DOAS white cell was equipped with narrow band dielectric mirrors (335–360 nm) for sensitive detection of BrO. Since the absorption cross section of OClO is within the same spectral range, this species might have been the measurable indicator for an activation of chloride. However, OClO remained below a mean detection limit of 150 ppt, and we may follow the simple relationship in Eq. (1) to calculate the contribution of bromine to the ozone loss to a value of 12 ppt s^{-1}. The difference to the observed ozone loss of 55 ppt s^{-1} might be caused by chlorine atoms, which were not monitored during the experiment. However, reaction constants leading to ozone loss due to chlorine (e.g. Reaction R10 and R12) and are much faster compared to bromine. It is well-known that an activation of bromide directly via mechanism Reactions (R6) and (R7) needs an acidification of the aqueous phase (e.g. Fickert et al., 1999). The NO_2 mixing ratio of 500 ppt must have been sufficient to activate the entire bromide via Reactions (R16)–(R18) or to form enough HNO_3 to provide the H^+ ions needed by Reaction (R7) via Reactions (R2) and (R3).

To decide about the dominant activation mechanism, we show a simulation run with the same starting conditions in Fig. 4. Herein plotted are the calculated mixing ratios of important trigger species vs. the total mixing ratio of gaseous Br_x species. The model plausibly reproduces the experiment in terms like the ozone decay, the BrO mixing ratio and the loss of NO_2. According to the model, a large fraction of bromide was activated directly through $BrNO_3$ hydrolysis (mechanism Reactions R16–R18 and R7). After the

ACPD
14, 10135–10166, 2014

NO_2 was nearly consumed, the activating mechanism changed to Reactions (R14), (R15) and (R7). This is indicated by proton consumption, causing an accelerated rise of the aerosol pH. With the model we might roughly quantify the extent of activated chlorine to a maximum of below 5 ppt ClO and below 3 ppt OClO. The main precursor of chlorine atoms was BrCl, which reached 2–4 ppt here, while the mixing ratio of Cl_2 (not shown), despite the lower photolysis frequency of Cl_2 in comparison to BrCl, was two orders of magnitude lower. Furthermore, Br_2 reached a plateau of about 40 ppt, while the peak of gaseous HOBr was around 70 ppt. The major precursor of HOBr, the HO_2 radical, had an almost constant, but slightly falling mixing ratio around 50 ppt, anti-correlated to HOBr. The total loss of methane could be calculated to 12 ppb. The main consumer of methane was the OH radical with its mixing ratio of 5–10 ppt, while chlorine atoms had a minor contribution here. One important oxidation product of methane is formaldehyde, since it is a main sink for bromine atoms to form HBr. The HCHO mixing ratio was calculated to be a plateau of 300 ppt. The high OH levels are explained by the low amounts of sinks in the surrounding air. Typical OH values in our chamber are below 0.5 ppt in a low NO_x case and between 0.5 and 2 ppt in a moderate NO_x atmosphere, measured by RCM with injected HCs.

3.2 High NO_x experiment with DOAS

As in the low NO_x experiment, we injected aerosol into a purged and humid chamber (55 % rel. humidity at 293 K) by nebulizing a stock solution containing 1 g L^{-1} NaCl and 86.4 mg L^{-1} NaBr. The aerosol reached a particle concentration of 1.8×10^4 cm^{-3} with a liquid water content of 5×10^{-10} $m^3\,m^{-3}$; its distribution is shown as curve B in Fig. 2. The bromide content of 300 mmol L^{-1} would allow a maximum Br_x-mixing ratio of 3.65 ppb, while the chloride content would allow a maximum Cl_x-mixing ratio of 78 ppb in the case of full halide activation. Figure 5 shows time profiles from this experiment, corresponding to a high-NO_x scenario. The dark chemistry started with an injection of 770 ppb O_3, causing the exponential loss of the previously constant NO_2 mixing ratio of 150 ppb. The solar simulator was switched on at minute −3, and the shutter was still

ACPD
14, 10135–10166, 2014

kept closed. Small light leaks around the shutter led already to a noticeable photolysis of NO_2 to NO. In daytime conditions, after opening the shutter at $t = 0$, the loss of NO_2 rapidly accelerated and the loss of ozone became slightly steeper. While NO_2 was still present, no halogen oxides could be observed within the statistical measurement error; however we assume that mechanism Reactions (R16)–(R18) was responsible for the NO_2 consumption. Once NO_2 was consumed, we observed a rapid acceleration of the ozone loss, which reached two noticeable maxima after 9.5 min ($-1.15\,ppb\,s^{-1}$) and 13 min ($-1.25\,ppb\,s^{-1}$). Both maxima can be related to different periods of halogen activation. The first is most likely caused by a high involvement of bromine atoms, indicated by an observed BrO mixing ratio of 764 ± 44 ppt (while the total BrO maximum of 841 ± 33 ppt was reached two minutes before). The ClO mixing ratio was 2770 ± 544 ppt at the first ozone depletion maximum with a rising tendency, reaching almost twice the value of 4114 ± 513 ppt at the point of the second ozone depletion maximum. The OClO mixing ratio time series with a maximum of 6907 ± 78 ppt in the middle of both ozone depletion maxima had a remarkable round shape. Since OClO is a direct reaction product of ClO and BrO (Reaction R12), its shape can be explained by the behavior of the precursors: the decrease of BrO and a coincident rise of ClO. The trapezoidal behavior of the BrO profile appears to be a consequence of stationary states involving its formation by consumption of ozone by atomic Br at the beginning and its consumption by self-reaction and reaction with ClO, forming OClO. After 18 min, the ozone was totally consumed, and the mixing ratios of the halogen oxides declined. A slight increase of the NO_2 mixing ratio to a plateau of 1.5 ppb was observed afterwards.

As well as in the low NO_x case, the model reasonably reproduces the experiment compared to most of the measured species (Fig. 6). The simulated mixing ratios of the halogen oxides species are quite comparable to the experiment, although the OClO values are lower. This may be caused by a higher supply of bromine in the experiment, probably by the chamber walls. The consumption of ozone starts at nighttime by the production of N_2O_5, which is heterogeneously converted to $ClNO_2$ and $BrNO_2$ on the particle surface (Reaction R19). The model calculates a total loss of bromide

ACPD
14, 10135–10166, 2014

following this pathway and a constant mixing ratio of 3.65 ppb of $BrNO_2$ after 100 s. Also a continued loss of chloride during nighttime by forming almost 30 ppb of $ClNO_2$ is predicted by the model. In daytime conditions both nitryl species are photolysed to X and NO_2. The halogen atoms react with ozone and NO_2 and produce XNO_3 according to Reaction (R16). The photodissociation of XNO_3 to X and NO_3 (Soller et al., 2002) leads to the photolytic steady state of N_2O_5 while NO_2 is available in gas phase. For X = Br, Reaction (R16) replenishes the bromide in the aerosol droplets by uptake and dissociation. In a comprehensive view, the sink for most NO_x and XNO_x species is the formation of nitrate in the droplets.

3.3 CIMS runs

A CIMS measurement may give information about the direct precursors of X, XO species, i.e. X_2 and XNO_2. We performed two experiments to demonstrate different mechanisms of halogen activation and conversion of active halogen species. Both experiments where done on a single day, causing some remaining reaction products and a fraction of old aerosol from the first experiment to influence the second run (see Fig. 6). In these early experiments the chamber was not cleaned before the chamber runs and thus contained HC and NO_x (which was converted to HONO on the droplet surface during the aerosol injection for the first run). After the injection of ozone into the dark chamber, we observed bromine in the gas phase (both isotopes in the correct mixing ratio of 50.7 %/49.3 %). Since this was a nighttime formation we assume the occurrence of mechanism Reactions (R4)–(R8). Such nighttime formed gaseous bromine may trigger the auto-catalytic halide activation cycles during dawn. In daytime conditions, we observed a rapid increase of the Br_2 mixing ratio, which reached its maximum of 6.1 ppb after 7 min of illumination. Cl_2 reached its maximum of 11.5 ppb 6 min later. Both maxima occurred while NO_x (originating from the photolysis of HONO) was still present in high mixing ratios. This verifies the calculation of the halogen species concentrations Cl_2 and Br_2 by the model in Fig. 5. The slight increase of $ClNO_2$ after the beginning of illumination is correlated with the production of N_2O_5 from the XNO_3

ACPD
14, 10135–10166, 2014

photolysis. A large fraction of Cl_2 (8.5 ppb) remained in the gas phase after the light was switched off. It caused a heterogeneous release of bromine (Reactions R20–R22) out of fresh aerosol, which was injected in preparation of the subsequent run. Also a production of HONO was observed during the aerosol injection period. There are several indicators for the occurrence of Reaction (R23): (A) the production of HONO halted with the stop of aerosol injection; Reaction (R23) provides chloride to the aerosol phase and can occur on non-saturated aerosol only. (B) The supply of chloride by Reaction (R23) during the particle generation must lead to bigger particles, which was observed after the aerosol injection for the second run. (C) The NO_x measurement by the CLD 700 instrument with the molybdenum NO_x-converter was constant (not shown), which indicates a 1 : 1-conversion and thus excludes the heterogeneous $2NO_2 + H_2O \rightarrow HONO + H^+ + NO_3^-$ reaction.

The relatively low CIMS-signals of both HO_x species and the high XO mixing ratios measured by DOAS led us to introduce the previously mentioned HOX to X + OH reactions.

4 Summary and conclusions

Generally speaking, the result of an experimental run is strictly dependent on the initial NO_x mixing ratio. An overview of this dependence is shown in Fig. 7, where the maximum ozone decay of 42 experimental runs is plotted vs. their initial NO_x-levels. Additionally shown are model runs with similar initial conditions. All of our experiments share a common chloride concentration in the stock solution and a common particle mean diameter. The main differences are their bromide content and the liquid water content. According to model calculations and experimental runs (full pink diamonds) the bromide content and the lwc affect the maximum ozone decay linearly in the regarded range. Even at bromide levels as low as 1.5 mmol L^{-1}, where the salt was taken from commercial road salt, a strong ozone depletion is observed. Most experiments without an addition of HC were carried out at a lwc of $\sim 5 \times 10^{-10}$. These follow

ACPD
14, 10135–10166, 2014

a logarithmic curve: $(d[O_3]/dt)_{max} = 0.223 \times \ln([NO_x]_{init} - 0.63$. The ozone loss depends strongly on of the initial nitrogen oxides mixing ratio as it is shown by the black fitting function in Fig. 7. Model runs with similar starting conditions (empty black dots) are in good agreement with the experiments at moderate and high NO_x values. Even at low NO_x values, the model predicts faster ozone decay (red fit). We explain this difference by HC impurities in the lower ppb range (< 10 ppb non-methane HC, measured by FID), since HCs slow down the ozone depletion by scavenging the halogens to HX and due to an ozone production of the RO_2 cycle. This can also be seen by injecting HCs (red dots). Following the model calculations one can define a noticeable release of chlorine in a ppt range from 0.5 ppb of NO_x, which results in an accelerated consumption of ozone. Moreover, this overview demonstrates characteristic differences between the activation in salt droplets and salt pans shown in Buxmann et al. (2012); additionally to the dependence on NO_x, the activation of halides from the solid phase is dependent on the liquid water layers on the crystals.

In all cases the activation of bromide was found to be preferred over chloride. An initial activation of bromide to Br_2 may occur already in the dark, driven by dissolved ozone. The acidification of the aerosol liquid phase is often provided by nitrogen oxides. However, the influence of NO_x on halogen activation is not restricted to acidification, but leads also to a heterogeneous release of photolabile reservoir species (i.e. NO_x, XNO_2, XNO_3) in the night and daytime; in high NO_x cases bromide and chloride is activated utterly by NO_x mechanisms. Although bromide eases the release of chloride due to the equilibrium between $Br_2 + Cl^-$ and $BrCl + Br^-$, the activation of chlorine is not necessarily dependent on the bromide concentration, as measurements on road salt showed. High NO_x experiments showed a strong activation of chloride even in cases where the concentration of bromide was in the lower millimolar range. Such conditions could be present on roads, which are de-iced by NaCl-salts in winter time; they are a possible source of continental $ClNO_2$. Furthermore, the presence of chlorine and bromine would have significant impact on the tropospheric ozone level as well as methane in highly polluted coastal regions. Only a few studies exist (e.g. Osthoff

ACPD
14, 10135–10166, 2014

et al., 2008; Phillips et al., 2012), which do not allow a global budget. Even though, amounts of tropospheric NO_2 has likely decreased by 30 to 50 % in Europe and North America, it has increased by more than a factor of 2 in Asia since the mid-1990 s (Hilboll et al., 2013), which might influence the total amount of reactive bromine and especially chlorine in the atmosphere, according to our findings. This should be further investigated in future studies.

Once NO_x is consumed, the mechanism changes to HOX and precedes the activation cycle via the protons provided by NO_x previously. The model in its current stage reasonably reproduces chamber experiments in terms of ozone loss and halogen activation and its dependence on NO_x. However, the influence of the chamber walls needs to be considered as a secondary liquid phase in the model in upcoming work.

Supplementary material related to this article is available online at http://www.atmos-chem-phys-discuss.net/14/10135/2014/acpd-14-10135-2014-supplement.pdf.

Acknowledgements. We would like to thank R. von Glasow, F. Siekmann and J. Wittmer for detailed discussions. We also thank the Deutsche Forschungsgemeinschaft for funding research unit 763.

References

Atkinson, R., Baulch, D. L., Cox, R. A., Crowley, J. N., Hampson, R. F., Hynes, R. G., Jenkin, M. E., Rossi, M. J., and Troe, J.: Evaluated kinetic and photochemical data for atmospheric chemistry: Volume III – gas phase reactions of inorganic halogens, Atmos. Chem. Phys., 7, 981–1191, doi:10.5194/acp-7-981-2007, 2007.

Balzer, N.: Kinetische Untersuchungen der Halogen-Aktivierung einer simulierten Salzpfanne in einer Smogkammer, Ph.D. thesis, University of Bayreuth, Bayreuth, Germany, 2012.

ACPD
14, 10135–10166, 2014

Behnke, W., Holländer, W., Koch, W., Nolting, F., and Zetzsch, C.: A smog chamber for studies of the photochemical degradation of chemicals in the presence of aerosols, Atmos. Environ., 22, 1113–1120, 1988.

Behnke, W., Scheer, V., and Zetzsch, C.: Formation of $ClNO_2$ and HNO_3 in the presence of N_2O_5 and wet pure NaCl and wet mixed $NaCl/Na_2SO_4$-aerosol, J. Aerosol Sci., 24, 115–116, 1993.

Behnke, W., George, C., Scheer, V., and Zetzsch, C.: Production and decay of $ClNO_2$ from the reaction of gaseous N_2O_5 with NaCl solution: bulk and aerosol experiments, J. Geophys. Res., 102, 3795–3804, 1997.

Behnke, W., Elend, M., Krüger, U., and Zetzsch, C.: The influence of NaBr/NaCl ratio on the Br^--catalysed production of halogenated radicals, J. Atmos. Chem., 34, 87–99, 1999.

Betts, R. H. and Mackenzie, A. N.: Formation and stability of hypobromous acid in perchloric acid solutions of bromine and bromate ions, Can. J. Chem., 29, 666–677, 1951.

Bleicher, S.: Zur Halogenaktivierung im deliquestzenten Aerosol und in Salzpfannen, Ph.D. thesis, University of Bayreuth, available at: http://opus4.kobv.de/opus4-ubbayreuth/files/1370/Bleicher+Diss.pdf (last access: 1 March 2014), 2012.

Buxmann, J.: Bromine and Chlorine Explosion in a Simulated Atmosphere, Ph.D. thesis, University of Heidelberg, Heidelberg, Germany, 2012.

Buxmann, J., Balzer, N., Bleicher, S., Platt, U., and Zetzsch, C.: Observations of bromine explosions in smog chamber experiments above a model salt pan, Int. J. Chem. Kinet., 44, 312–326, 2012.

Cox, R. A. and Lewis, R.: Kinetics of chlorine oxide radical reactions using modulated photolysis, Part 3. – Pressure and temperature dependence of the reaction: $ClO + NO_2(+M) \rightarrow ClONO_2(+M)$, J. Chem. Soc. Faraday T., 1, 75, 2649–2661, 1979.

da Rosa, M. and Zetzsch, C.: Influence of pH and halides on halogen species in the aqueous phase, J. Aerosol Sci., 32, S311–S312, 2001.

Deiber, G., George, Ch., Le Calvé, S., Schweitzer, F., and Mirabel, Ph.: Uptake study of $ClONO_2$ and $BrONO_2$ by Halide containing droplets, Atmos. Chem. Phys., 4, 1291–1299, doi:10.5194/acp-4-1291-2004, 2004.

DeMore, W. B., Sander, S. P., Golden, D. M., Hampson, R. F., Kurylo, M. J., Howard, C. J., Ravishankara, A. R., Kolb, C. E., and Molina, M. J.: Chemical kinetics and photochemical data for use in stratospheric modeling, Evaluation number 12, JPL Publication 97-4, Jet Propulsion Laboratory California Institute of Technology Pasadena, California, 1–266, 1997.

ACPD
14, 10135–10166, 2014

Fickert, S., Adams, J. W., and Crowley, J. N.: Activation of Br_2 and BrCl via uptake of HOBr onto aqueous salt solutions, J. Geophys. Res., 104, 23719–23727, 1999.
Finlayson-Pitts, B. J.: Reaction of NO2 with NaCl and atmospheric implications of NOCl formation, Nature, 306, 676–677, 1983.
Finlayson-Pitts, B. J., Ezell, M. J., Pitts Jr., J. N.: Formation of chemically active chlorine compounds by reactions of atmospheric NaCl particles with gaseous N_2O_5 and $ClONO_2$, Nature, 337, 241–244, 1989.
Frenzel, A., Scheer, V., Sikorski, R., George, C., Behnke, W., and Zetzsch C.: Heterogeneous interconversion reactions of $BrNO_2$, $ClNO_2$, Br_2, and Cl_2, J. Phys. Chem. A, 102, 1329–1337, 1998.
George, C., Ponche, J. L., Mirabel, P., Behnke, W., Scheer, V., and Zetzsch, C.: Study of the uptake of N_2O_5 by water and NaCl solutions, J. Phys. Chem., 98, 8780–8784, 1994.
Hanson, D. R., Ravishankara, D. R., and Lovejoy, E. R.: Reaction of $BrONO_2$ with H_2O on submicron sulfuric acid aerosol and the implications for the lower stratosphere, J. Geophys. Res., 101, 9063–9069, 1996.
Hippler, H., Krasteva, N., Nasterlack, S., and Striebel, F.: Reaction of OH + NO_2: high pressure experiments and falloff analysis, J. Phys. Chem. A, 110, 6781–6788, 2006.
Hilboll, A., Richter, A., and Burrows, J. P.: Long-term changes of tropospheric NO_2 over megacities derived from multiple satellite instruments, Atmos. Chem. Phys., 13, 4145–4169, doi:10.5194/acp-13-4145-2013, 2013.
Hoch, D. J., Buxmann, J., Sihler, H., Pöhler, D., Zetzsch, C., and Platt, U.: An instrument for measurements of BrO with LED-based Cavity-Enhanced Differential Optical Absorption Spectroscopy, Atmos. Meas. Tech., 7, 199–214, doi:10.5194/amt-7-199-2014, 2014.
Hunt, S. W., Roeselová, M., Wang, W., Wingen, L. M., Knipping, E. M., Tobias, D. J., Dabdub, D., and Finlayson-Pitts, B. J.: Formation of molecular bromine from the reaction of ozone with deliquesced NaBr aerosol: evidence for interface chemistry, J. Phys. Chem. A, 108, 11559–11572, 2004.
Kercher, J. P., Riedel, T. P., and Thornton, J. A.: Chlorine activation by N_2O_5: simultaneous, in situ detection of $ClNO_2$ and N_2O_5 by chemical ionization mass spectrometry, Atmos. Meas. Tech., 2, 193–204, doi:10.5194/amt-2-193-2009, 2009.
Liao, J., Sihler, H., Huey, L. G., Neuman, J. A., Tanner, D. J., Friess, U., Platt, U., Flocke, F. M., Orlando, J. J., Shepson, P. B., Beine, H. J., Weinheimer, A. J., Sjostedt, S. J., Nowak, J. B., Knapp, D. J., Staebler, R. M., Zheng, W., Sander, R., Hall, S. R., and Ullmann, K.:

ACPD
14, 10135–10166, 2014

A comparison of Arctic BrO measurments by chemical ionization mass spectrometry and long path-differential optical absorbtion spectroscopy, J. Geophys. Res., 116, D00R02, doi:10.1029/2010JD014788, 2011.

Lopez-Hilfiker, F. D., Constantin, K., Kercher, J. P., and Thornton, J. A.: Temperature dependent halogen activation by N_2O_5 reactions on halide-doped ice surfaces, Atmos. Chem. Phys., 12, 5237–5247, doi:10.5194/acp-12-5237-2012, 2012.

Madronich, S. and Flocke, S.: The role of solar radiation in atmospheric chemistry, in: The Handbook of Enviromental Chemistry, vol. 2, Part I: Environmental Photochemistry, edited by: Boule, P., Springer, Berlin, 1–26, 1999.

Maric, D., Burrows, J. P., Meller, R., and Moortgat, G. K.: Visible absorption spectra of molecular chlorine, J. Photochem. Photobiol. A, 70, 205–214, 1993.

Morris, J. C.: The acid ionization constant of HOCl from 5 to 35°, J. Phys. Chem., 70, 3798–3805, 1966.

Palm, W.-U., Elend, M., Krüger, H.-U., and Zetzsch, C.: OH radical reactivity of airborne terbuthylazine adsorbed on inert aerosol, Environ. Sci. Technol., 31, 3389–3396, 1997.

Neuman, J. A., Nowak, J. B., Huey, L. G., Burkholder, J. B., Dibb, J. E., Holloway, J. S., Liao, J., Peischl, J., Roberts, J. M., Ryerson, T. B., Scheuer, E., Stark, H., Stickel, R. E., Tanner, D. J., and Weinheimer, A.: Bromine measurements in ozone depleted air over the Arctic Ocean, Atmos. Chem. Phys., 10, 6503–6514, doi:10.5194/acp-10-6503-2010, 2010.

Osthoff, H. D., Roberts, J. M., Ravishankara, A. R., Williams, E. J., Lerner, B. M., Sommariva, R., Bates, T. S., Derek Coffman, D., Quinn, P. K., Dibb, J. E., Stark, H., Burkholder, J. B., Talukdar, R. K., Meagher, J., Fehsenfeld, F. C., and Brown, S. S.: High levels of nitryl chloride in the polluted subtropical marine boundary layer, Nat. Geosci., 1, 324–328, 2008.

Peters, C., Pechtl, S., Stutz, J., Hebestreit, K., Hönninger, G., Heumann, K. G., Schwarz, A., Winterlik, J., and Platt, U.: Reactive and organic halogen species in three different European coastal environments, Atmos. Chem. Phys., 5, 3357–3375, doi:10.5194/acp-5-3357-2005, 2005.

Phillips, G. J., Tang, M. J., Thieser, J., Brickwedde, B., Schuster, G., Bohn, B., Lelieveld, J., and Crowley, J. N.: Significant concentrations of nitryl chloride observed in rural continental Europe associated with the influence of sea salt chloride and anthropogenic emissions, Geophys. Res. Lett., 39, L10811, doi:10.1029/2012GL051912, 2012.

ACPD
14, 10135–10166, 2014

Platt, U. and Janssen, C.: Observation and role of the free radicals NO_3, ClO, BrO and IO in the troposphere, Faraday Discuss., 100, 175–198, 1995.
Pratt, K. A., Custard, K. D., Shepson, P. B., Douglas, T. A., Pöhler, D., General, S., Zielcke, J., Simpson, W. R., Platt, U., Tanner, D. J., Huey, G. L., Carlsen, M., and Stirm, B. H.: Photochemical production of molecular bromine in Arctic surface snowpacks, Nat. Geosci., 6, 351–356, 2013.
Rossi, M. J.: Heterogeneous reactions on salts, Chem. Rev., 103, 4823–4882, 2003.
Sander, R., Baumgaertner, A., Gromov, S., Harder, H., Jöckel, P., Kerkweg, A., Kubistin, D., Regelin, E., Riede, H., Sandu, A., Taraborrelli, D., Tost, H., and Xie, Z.-Q.: The atmospheric chemistry box model CAABA/MECCA-3.0, Geosci. Model Dev., 4, 373–380, doi:10.5194/gmd-4-373-2011, 2011.
Sander, S. P., Ray, G. W., and Watson, R. T.: Kinetics study of the pressure dependence of the BrO + NO_2 reaction at 298 Kelvin, J. Phys. Chem., 85, 199–210, 1981.
Scheer, V., Frenzel, A., Behnke, W., Zetzsch, C., Magi, L., George, C., and Mirabel, P.: Uptake of nitrosyl chloride (NOCl) by aqueous solutions, J. Phys. Chem. A, 101, 9359–9366, 1997.
Schütze, M. and Herrmann, H.: Determination of phase transfer parameters for the uptake of HNO_3, N_2O_5 and O_3 on single aqueous drops, Phys. Chem. Chem. Phys., 4, 60–67, 2002.
Shilov, E. A.: On the calculation of the dissociation constants of hypohalogenous acids from kinetic data, J. Am. Chem. Soc., 60, 490–491, 1938.
Soller, R., Nicovich, J. M., and Wine, P. H.: Bromine nitrate photochemistry: quantum yields for O, Br, and BrO over the wavelength range 248–355 nm, J. Phys. Chem., 106, 8378–8385, 2002.
Thornton, J. A., Kercher, J. P., Riedel, T. P., Wagner, N. L., Cozic, J., Holloway, J. S., Dube, W. P., Wolfe, G. M., Quinn, P. K., Middlebrook, A. M., Alexander, B., and Brown, S. S.: A large atomic chlorine source inferred from midcontinental reactive nitrogen chemistry, Nature, 464, 271–274, 2010.
Wex, H., Kiselev, A., Stratmann, F., Zoboki, J., and Brechtel, F.: Measured and modeled equilibrium sizes of NaCl and $(NH_4)_2SO_4$ particles at relative humidities up to 99.1 %, J. Geophys. Res., 110, D21212, doi:10.1029/2004JD005507, 2005.
Wren, S. N., Donaldson, D. J., and Abbatt, J. P. D.: Photochemical chlorine and bromine activation from artificial saline snow, Atmos. Chem. Phys., 13, 9789–9800, doi:10.5194/acp-13-9789-2013, 2013.

ACPD
14, 10135–10166, 2014

Zetzsch, C. and Behnke, W.: Heterogeneous photochemical sources of atomic Cl in the troposphere, Ber. Bunsen. Phys. Chem., 96, 488–493, 1992.

ACPD
14, 10135–10166, 2014

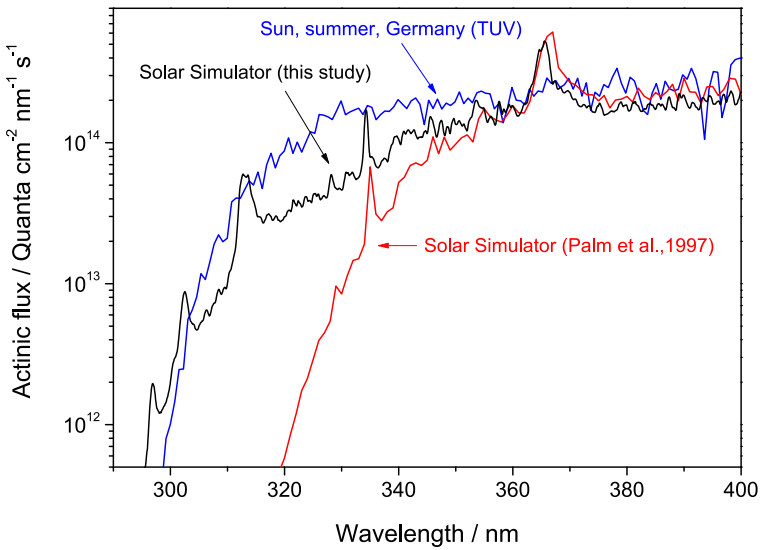

Fig. 1. Measured actinic photon flux in comparison to the sun in mid summer in Germany, calculated by Tropospheric Ultraviolet & Visible Radiation Model (TUV, Madronich and Flocke, 1999) and to a previous publication (Palm et al., 1997) with a glass filter that had been in use for 15 years. The glass filter is subject to solarization, which moves the UV-cutoff to red.

ACPD
14, 10135–10166, 2014

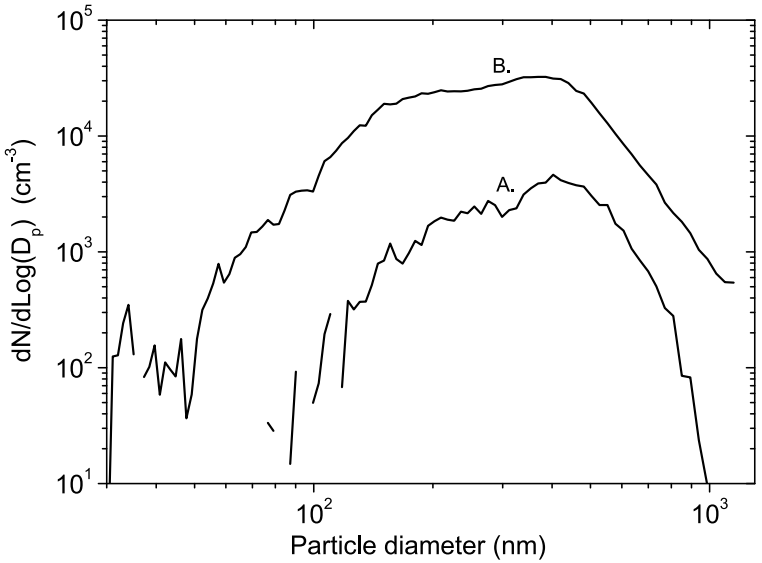

Fig. 2. Initial particle size distributions of the experiments discussed below. Both aerosols were generated from the same stock solution of $1\,g\,L^{-1}$ NaCl and $86.4\,mg\,L^{-1}$ NaBr, resulting in a common maximum at nearly at 400 nm. Run A was one of the first aerosol experiments with the DOAS instrument, where the particle concentration was kept lower to test the light loss by the Mie scattering. The content of liquid water was thus lower in run A (7×10^{-11}) compared to run B (5×10^{-10}).

ACPD
14, 10135–10166, 2014

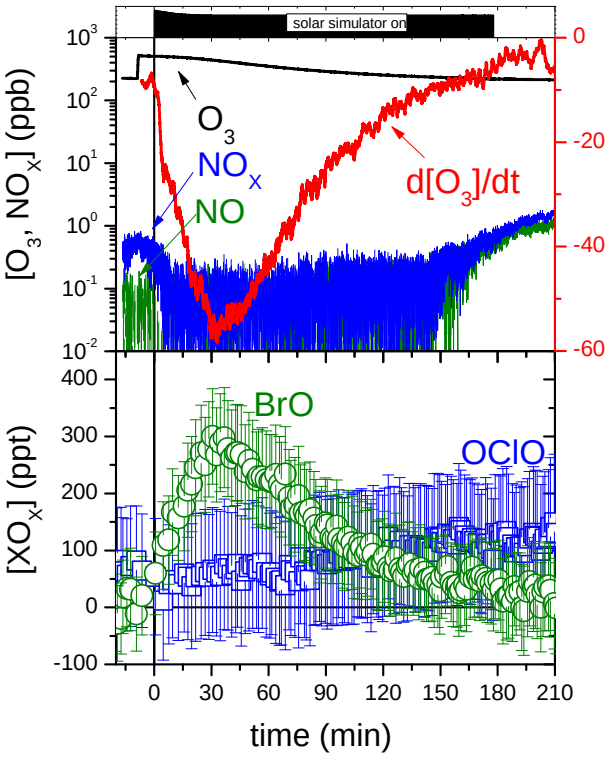

Fig. 3. Activation of bromide and its impact on ozone in a low NO_x scenario. A part of the BrO mixing ratio (200 ppt) was subtracted as an artifact from the previous chamber purge, since it was stable under night time conditions.

ACPD
14, 10135–10166, 2014

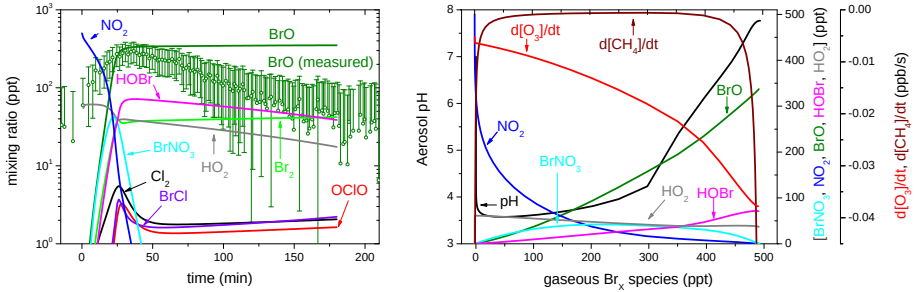

Fig. 4. Model calculation of the experiment shown in Fig. 3. Time profiles are plotted in the left figure, while in the right figure the data of the first 30 min is plotted against the gained gaseous Br_x species coming from the loss of bromide of the liquid phase. The modeled BrO reaches a stationary state at 350 ppt after 35 min with a slower decrease than the experiment and confirms a low level of OClO of 3 ppt, well below the detection limit of the DOAS instrument. The change of the activation regime during "day time" from $BrNO_3$ to HOBr after the NO_2 has almost completely been consumed and is indicated by a fast consumption of protons as it can be seen in the right figure.

ACPD
14, 10135–10166, 2014

Influence of NO_x on the activation of BrO and ClO in salt aerosol

S. Bleicher et al.

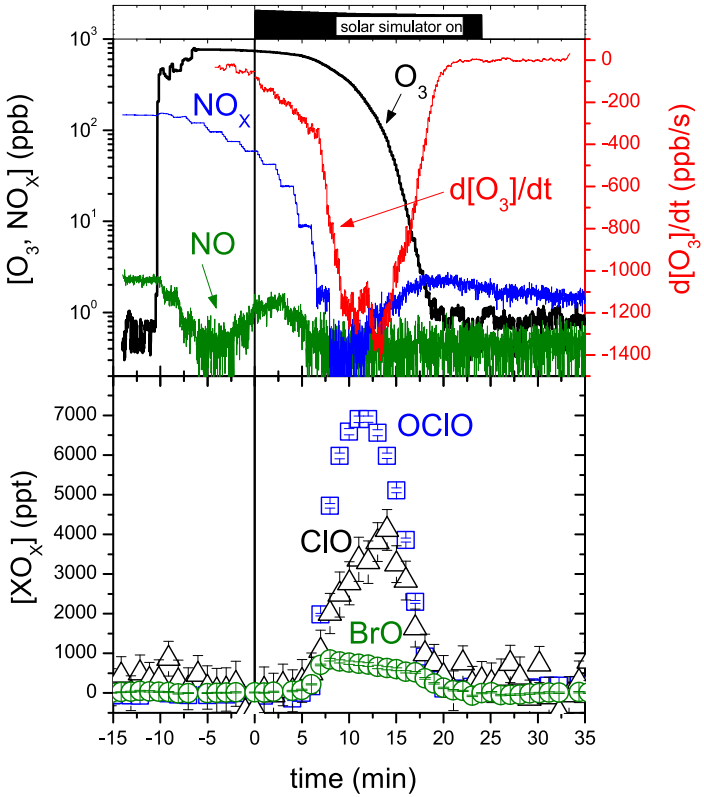

Fig. 5. High NO_x scenario with a large activation of chloride. The loss of NO_2 begins in the dark and can be explained by the production of N_2O_5 and XNO_2. A rapid loss of ozone was observed after the consumption of NO_2 under light conditions, thus forming the observable XO_x species. The remarkable round shape of OClO can be explained by the time profiles of its precursors BrO and ClO, which are both trapezoids.

ACPD
14, 10135–10166, 2014

Influence of NO_x on the activation of BrO and ClO in salt aerosol

S. Bleicher et al.

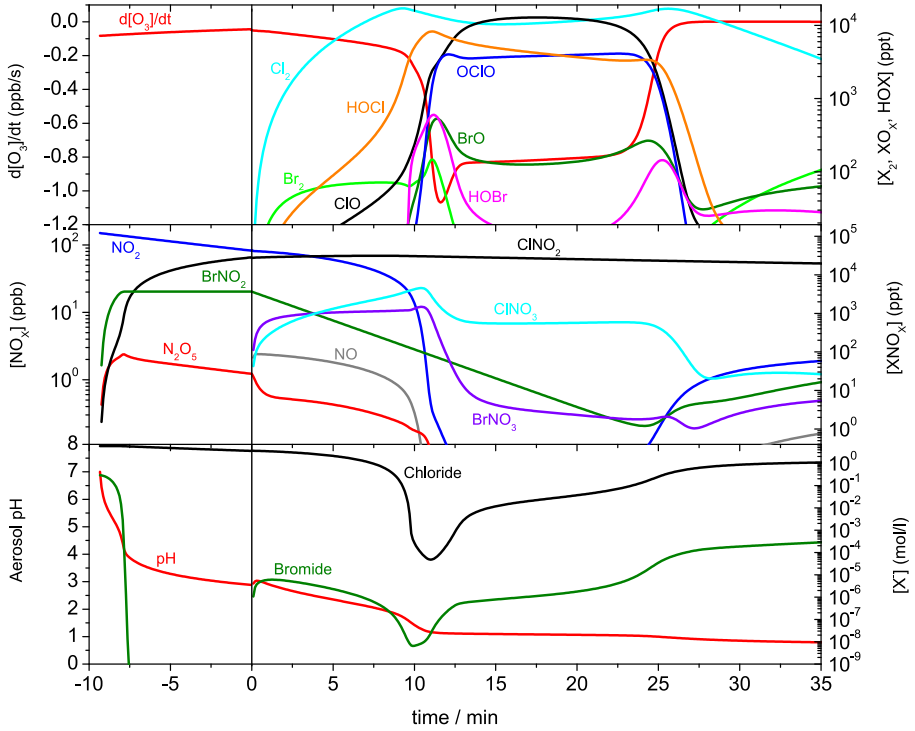

Fig. 6. Model calculation of halogen activation in a high NO_x scenario. Although the values of ozone depletion are comparable to the experiment, the simulation is 3–5 min delayed. This can be explained with wall sources from previous experiments. A higher simulated content of bromide in the liquid phase would explain a faster consumption of ozone and higher OClO mixing ratios as observed. In the logarithmic scale is the photolysis of $ClNO_2$ almost imperceptible: the $ClNO_2$ mixing ratio raises right after the day time conditions are switched on while NO_x is still available and declines after with its photolytic life time of $3 \times 10^{-4}\ s^{-1}$.

ACPD
14, 10135–10166, 2014

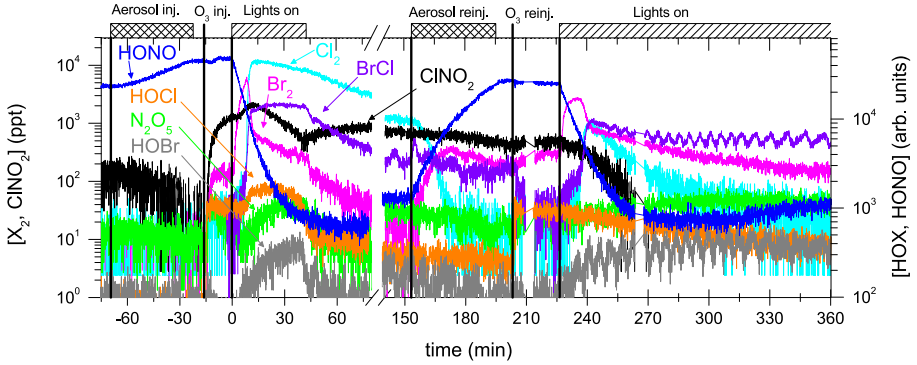

Fig. 7. CIMS measurement of HONO and the direct precursors of BrO (Br_2 and HOBr) and ClO (Cl_2, $ClNO_2$ and HOCl). The chamber contained a sum of 25 ppb of HONO and NO_x from ambient air impurities. During the aerosol injection, NO_x was heterogeneously converted to HONO. Its decay during daytime conditions suits the measured photolysis frequency of $j(\mathrm{HONO}) = 2\times10^{-3}\,\mathrm{s}^{-1}$. The maximum values of Br_2 and Cl_2 were reached while NO_x as a product of HONO.

ACPD
14, 10135–10166, 2014

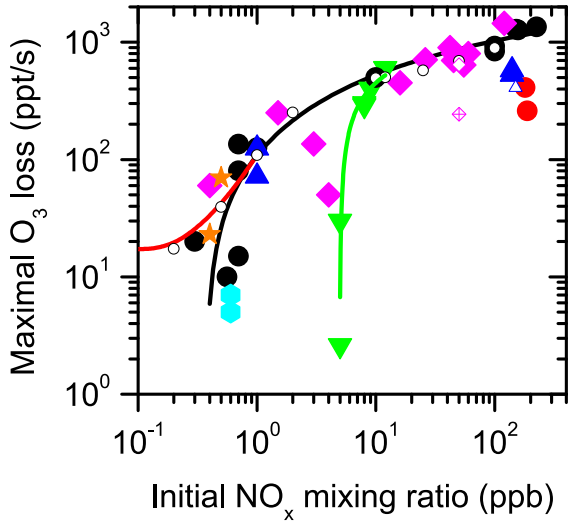

Fig. 8. Dependence of the maximum ozone loss on the initial NO_x concentration for 1 g L^{-1} NaCl aerosol with different bromide contents and variations of other parameters. The full symbols are experiments: black circles – 0.3 mol L^{-1} bromide and lwc 5×10^{-10}, red circles – 0.3 mol L^{-1} bromide and lwc 5×10^{-10} and additional VOC injected, blue triangles – 1.5 mmol L^{-1} (road salt) bromide and lwc 5×10^{-10}, green triangles – salt pan experiments from Buxmann et al., 2012, pink diamonds – 0.03 mol L^{-1} bromide and lwc 5×10^{-9}, cyan dots – 5.2 mmol L^{-1} bromide and lwc 5×10^{-9}, orange asterisks – 52 mmol L^{-1} bromide and lwc 5×10^{-9}. The open symbols are model runs with initial parameters corresponding to the experiments. The black curve was fitted to the full black circles, while the red curve was fitted to the open black circles. In the low range the model differs from the experiment due to VOC impurities in the zero air which slow down the halogen chemistry. The salt pan experiments are slowed down due to low rel. humidity.

ACPD
14, 10135–10166, 2014

Influence of NO_x on the activation of BrO and ClO in salt aerosol

S. Bleicher et al.